

## Two regimes of ionization-induced recovery in SrTiO<sub>3</sub> under irradiation

William J. Weber<sup>a,b,\*</sup>, Haizhou Xue<sup>a</sup>, Eva Zarkadoula<sup>b</sup>, Yanwen Zhang<sup>b,a</sup>

<sup>a</sup>Department of Materials Science & Engineering, University of Tennessee Knoxville, TN 37996, USA

<sup>b</sup>Materials Science & Technology Division, Oak Ridge National Laboratory, Oak Ridge, TN 37831, USA

\*William J. Weber; [wjweber@utk.edu](mailto:wjweber@utk.edu); Department of Materials Science & Engineering, 1508 Middle Drive, University of Tennessee, Knoxville, TN 37996, USA

### ABSTRACT

Irradiation of pre-damaged SrTiO<sub>3</sub> with 2 MeV He, 1.2 MeV C, 5 MeV C and 12 MeV O ions reveals two regimes of ionization-induced recovery. For C and O ions, with electronic energy loss between 1.6 and 3 keV/nm, recovery cross sections range from 0.27 to 0.38 nm<sup>2</sup>, and molecular dynamics confirms recovery related to ionization-induced thermal spikes via electron-phonon coupling. At lower electronic energy losses, recovery cross sections decrease to about 5.5×10<sup>-4</sup> nm<sup>2</sup> for 2 MeV He ions and 1.0×10<sup>-5</sup> nm<sup>2</sup> for 200 keV electrons, which suggests recovery associated with local electronic excitation processes.

Keywords: Rutherford backscattering spectrometry/channeling (RBS); Recovery; Perovskite; Defects; Molecular dynamics

*This manuscript has been authored by UT-Battelle, LLC under Contract No. DE-AC05-00OR22725 with the U.S. Department of Energy. The United States Government retains and the publisher, by accepting the article for publication, acknowledges that the United States Government retains a non-exclusive, paid-up, irrevocable, world-wide license to publish or reproduce the published form of this manuscript, or allow others to do so, for United States Government purposes. The Department of Energy will provide public access to these results of federally sponsored research in accordance with the DOE Public Access Plan (<http://energy.gov/downloads/doe-public-access-plan>).*

Electron and ion beams are widely used in the analysis, modification and functionalization of materials, as well as for emulating both natural and man-made radiation environments. While it is well-established that atomic-level defects are created by elastic energy transfer from charged particles to atomic nuclei (nuclear energy loss,  $S_n$ ), the effects of energy loss to target electrons (electronic energy loss,  $S_e$ ) is more complicated, particularly in complex oxides [1-4]. Strontium titanate ( $\text{SrTiO}_3$ ) is an important electro-optical material for multifunctional oxide electronics [5-8], and ion-beam irradiation can be utilized to tune its electro-optical properties [9-13]. As a functional ferroelectric material,  $\text{SrTiO}_3$  and related oxide perovskites have device applications in harsh nuclear and space radiation environments [14,15], and they have also been proposed for the immobilization of nuclear waste [16]. As a model transition metal oxide with the cubic perovskite structure,  $\text{SrTiO}_3$  provides critical insights for understanding the response of other oxides to ion irradiation effects and ion-beam processing.

It is well-established that accumulation of irradiation-induced defects due to  $S_n$  can lead to amorphization in  $\text{SrTiO}_3$  [3,16-18]. However, high-energy ions with  $S_e$  values above a threshold of  $\sim 6.5$  keV/nm interact synergistically with pre-existing defects in  $\text{SrTiO}_3$  to form amorphous nanotracks along ion trajectories at 300 K [19,20], and ions with  $S_e$  values exceeding 10 keV/nm form discontinuous amorphous tracks in pristine  $\text{SrTiO}_3$  [20,21,22]. It has been reported that  $S_e$  for incident ions at 300 K can affect the dynamics of defect evolution due to  $S_n$  [23]. Ion beam induced epitaxial recrystallization of amorphous  $\text{SrTiO}_3$  above 375 K has been reported and attributed to diffusion of irradiation-induced defects [24]. In contrast, recrystallization of

amorphous SrTiO<sub>3</sub> at 300 K under 200 keV electron irradiation has been reported [25]. While high energy ions contribute to damage production above a S<sub>e</sub> threshold of ~6.5 keV/nm, the effects of ionization below this threshold on damage evolution have not been studied, which may unravel the contrasting observations above. The present study addresses the separate effects of S<sub>e</sub> values below this threshold on damage evolution in pre-damaged SrTiO<sub>3</sub> at 300 K using He, C and O ions, and the results reveal two distinct regimes of ionization-induced recovery.

This study used epi-polished, <100>-oriented, single crystal SrTiO<sub>3</sub> wafers obtained from the MTI Corp (<https://www.mtixtl.com/>). Ion irradiations and *in situ* characterization by Rutherford backscattering spectrometry in channeling geometry (RBS/C) were performed using the capabilities within the Ion Beam Materials Laboratory at the University of Tennessee [26]. A pre-damaged state was introduced by irradiation with 0.9 MeV Au ions at 300 K to a fluence of 6.4×10<sup>13</sup> ions/cm<sup>2</sup> at a flux of 4.2×10<sup>11</sup> ions/cm<sup>2</sup>s, which created a relative peak disorder of ~0.72 on the Sr sublattice, as measured by RBS/C. The concentration of implanted Au atoms was less than 0.1 at%, which limited chemical effects and lattice distortions from implanted Au. These pre-damaged samples were subsequently irradiated over a range of ion fluences with 1.2 MeV C ions (S<sub>e</sub> = 1.60 keV/nm), 5.0 MeV C ions (S<sub>e</sub> = 2.27 keV/nm), and 12 MeV O ions (S<sub>e</sub> = 3.01 keV/nm) at ion fluxes of 1-2×10<sup>12</sup> ions/cm<sup>2</sup>s for C ions and 5×10<sup>11</sup> ions/cm<sup>2</sup>s for O ions. Disorder recovery in these samples with increasing ion fluence was characterized *in situ* by RBS/C using 3.5 MeV He ions (S<sub>e</sub> = 0.32 keV/nm). To investigate the response of pre-damaged SrTiO<sub>3</sub> to even lower values of S<sub>e</sub>, an additional pre-damaged state was created by irradiation

with 0.6 MeV Au ions to a fluence  $2.5 \times 10^{13}$  ions/cm<sup>2</sup> at a flux of  $2.1 \times 10^{11}$  ions/cm<sup>2</sup>s, which resulted in a lower relative peak disorder of 0.53 that should be more susceptible to annealing [27]. This pre-damaged sample was irradiated with 2 MeV He ions ( $S_e = 0.43$  keV/nm) at a flux of  $4.3 \times 10^{12}$  ions/cm<sup>2</sup>s, and the recovery was measured by continuous collection of RBS/C spectra, which were saved at periodic intervals.

All irradiations and RBS/C analyses were carried out in high vacuum ( $< 1.0 \times 10^{-7}$  Torr) at 300 K. Because of low ion fluxes, the temperature increase due to the ion beam was less than 10 K. Stopping powers and ion ranges were predicted by the SRIM 2008 code [28,29], assuming a density of 5.118 g/cm<sup>3</sup>.

Molecular dynamics (MD) simulations, combined with the inelastic thermal spike model [30], were used to model the response of pre-damaged SrTiO<sub>3</sub> to the dissipation of  $S_e$  along the path of 12 MeV O ions. The inelastic thermal spike model is based on the two-temperature model that describes the transfer of  $S_e$  from a fast ion to the atomic lattice via electron-phonon coupling. As described in detail previously for SrTiO<sub>3</sub> [3,31,32], the inelastic thermal spike model calculates the profile of energy transferred to the lattice for an ion of given energy, and this energy profile is used as input to MD simulations for each thermal spike event.

The DL POLY code [33] was used, with empirical potentials by McCoy et al. [34] joined to ZBL [28] repulsive potentials for short distances. The pre-damaged state was created by introducing 3% Frenkel pairs randomly into the simulation cell. The system contained 100860 atoms and was initially equilibrated under the constant pressure and temperature ensemble for 50

**Table 1**

Corresponding electronic energy loss,  $S_e$ , and ionization-induced recovery cross section,  $\sigma_r$ , for different charged particles used to irradiate pre-damaged SrTiO<sub>3</sub>.

Particle/Energy	$S_e$ (keV/nm)	$S_n$ (keV/nm)	$\sigma_r$ (nm <sup>2</sup> )
12 MeV O ions	3.01	0.0045	$0.38 \pm 0.02$
5 MeV C ions	2.27	0.0042	$0.32 \pm 0.02$
1.2 MeV C ions	1.60	0.013	$0.27 \pm 0.01$
2 MeV He ions	0.43	0.00042	$5.5 \times 10^{-4} \pm 6 \times 10^{-5}$
200 keV electrons	0.001		$1.0 \times 10^{-5} \pm 1 \times 10^{-6}$

ps. Forty thermal spike events were simulated under the microcanonical (NVE) ensemble, using a variable timestep. The incident direction for each thermal spike was along the z direction, and thermal spikes were randomly initiated within a 3 nm x 3 nm projected area. Energy scaling was used within 1 nm width of the cell boundaries, along the x and y directions, to emulate energy dissipation in the bulk. The simulation time for each thermal spike (~10 ps) was sufficient to cool down the system before the next event was initiated.

Samples pre-damaged with 0.9 MeV Au ions exhibit a peak in relative disorder at a depth of 100 nm, while those pre-damaged with 0.6 MeV Au ions exhibited a disorder peak at 70 nm. For the He, C and O ions, the ion ranges are much deeper (several  $\mu\text{m}$ ), and the accumulation of implanted He, C and O atoms has negligible impact on the pre-damaged region. The high ratio of electronic to nuclear energy loss,  $S_e/S_n$  (>50), and low values of  $S_n$  predicted by the SRIM code for He, C and O ions over the pre-damaged depth (see Table 1) limits their contribution to the

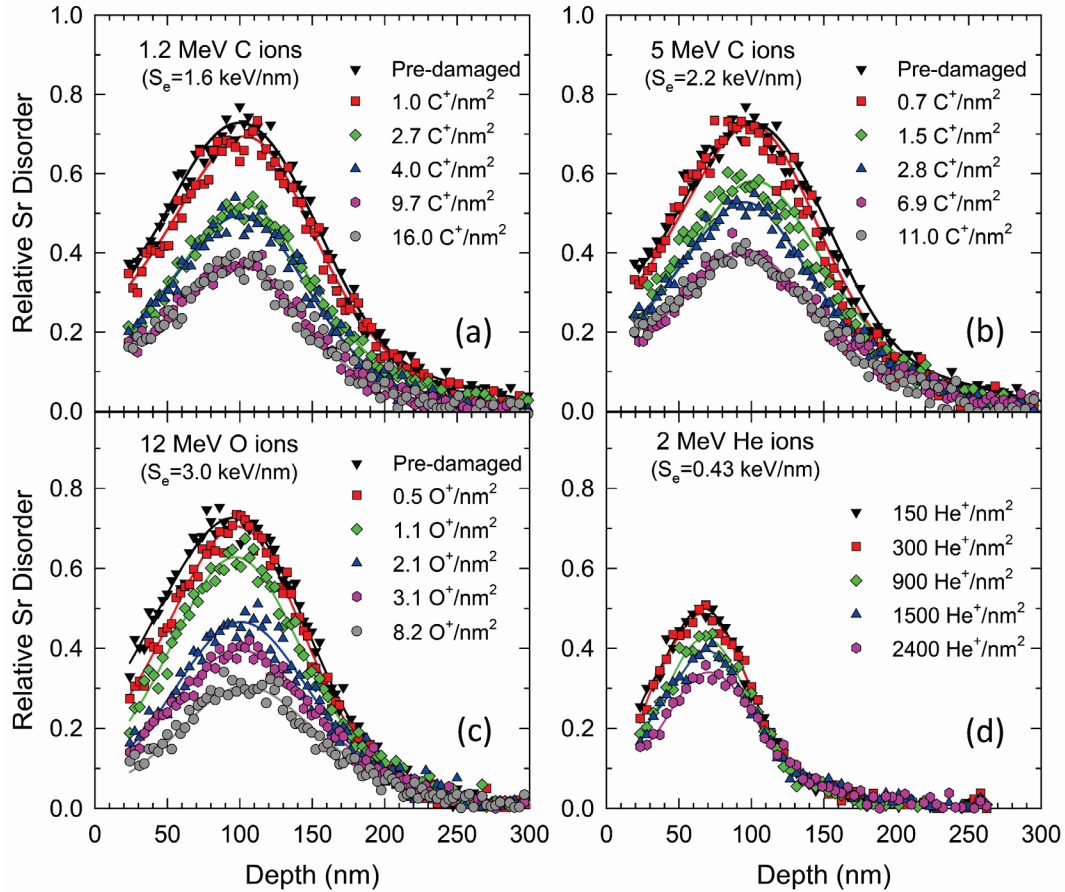


**Fig. 1.** Relative Sr disorder as a function of depth for pre-damaged SrTiO<sub>3</sub> irradiated to different ion fluences using different ions: (a) 1.2 MeV C ions; (b) 5 MeV C ions; (c) 12 MeV O ions; and (d) 2 MeV He ions. For simplicity, not all ion fluences are shown for the 12 MeV O ion and 2 MeV He ion irradiations.

measured disorder over this depth.

An iterative procedure originally developed for SrTiO<sub>3</sub> [18] was employed to determine the depth profiles of the relative disorder from the RBS/C spectra, where a relative disorder of 1.0 refers to a random or fully amorphous state and 0 refers to the undamaged pristine crystal. The results for 1.2 MeV C, 5 MeV C, 12 MeV O and 2 MeV He ions are shown in Fig. 1. For the C

and O ion irradiations, the initial pre-damaged disorder maximum was  $\sim 0.72$ , and the decrease in relative disorder with increasing ion fluence is clearly evident across the pre-damaged depth. The low  $S_e$  value of 3.5 MeV He ions used for RBS/C minimized any ionization-induced recovery during RBS/C measurements of the C and O ion irradiated samples. For both 1.2 and 5 MeV C ions, recovery tends to level off at a relative disorder level of 0.4, as shown in Fig. 1(a) and (b). The higher  $S_e$  for 12 MeV O ions leads to more recovery, as illustrated in Fig. 1(c). Due to a higher  $S_e$ , 2 MeV He ions were used to quantify damage recovery. The slightly lower pre-damaged disorder ( $\sim 0.53$ ) is not expected to affect the analysis, and the initial disorder profile measured with 2 MeV He ions corresponds to a fluence of 150 He ions/nm<sup>2</sup>, as shown in Fig. 1(d), which is considered representative of the actual pre-damaged state. While RBS/C spectra were collected after each incremental fluence of 150 He ions/nm<sup>2</sup>, only a subset of derived disorder depth profiles are shown in Fig. 1(d). Measurable recovery is not observed until a fluence of 450 He ions/nm<sup>2</sup>.

The normalized recovery of relative disorder at the damage peak is described by  $N/N_0$ , where  $N$  is the relative peak disorder for a given fluence and  $N_0$  is the initial pre-damaged peak disorder. The normalized recoveries with increasing ion fluence are shown in Fig. 2 and follow a simple exponential decrease with increasing ion fluence,  $\phi$ , given by the expression:

$$N/N_0 = 1 - N_r/N_0 [1 - \exp(-\sigma_r\phi)], \quad (1)$$

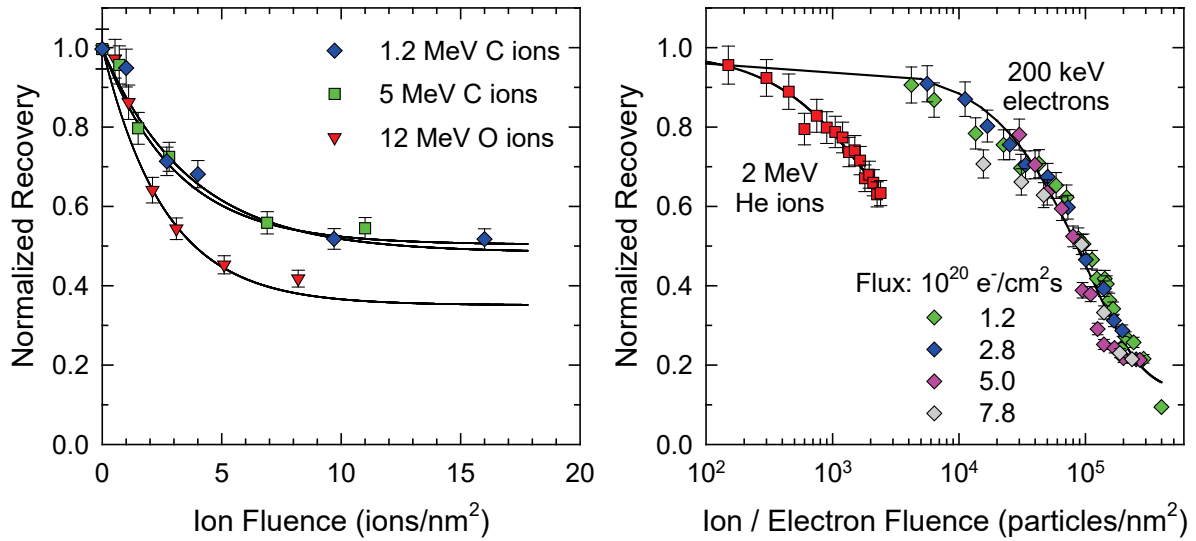


**Fig. 2.** Normalized recovery as a function of fluence for pre-damaged SrTiO<sub>3</sub>: (a) 1.2 and 5 MeV C ions and 12 MeV O ions; (b) 2 MeV He ions (squares) and 200 keV electrons (diamonds) at different electron fluxes. Solid curves are fits of Eq. (1) to the data. The electron recovery data are derived from an earlier study [25].

where  $N_r/N_0$  is the recoverable fraction of disorder and  $\sigma_r$  is the recovery cross section. A fit of Eq. (1) to the data in Fig. 2 yields the recovery cross sections, which are given in Table 1. The different initial disorder levels (C and O ions vs He ions) may affect the derived cross sections, but previous studies on SiC suggest negligible effects [35]. Included in Fig. 2(b) is the normalized recovery, derived from an earlier study [25], of pre-damaged SrTiO<sub>3</sub> due to 200 keV electron irradiation at different electron fluxes, along with a fit of Eq. (1) to the data. The electron-beam induced recovery, which as an activation energy of 0.1 eV [25] does not exhibit any clear dependence on electron flux within the narrow range from 1.2 to  $7.9 \times 10^{20} \text{ e}^-/\text{cm}^2\text{s}$ .

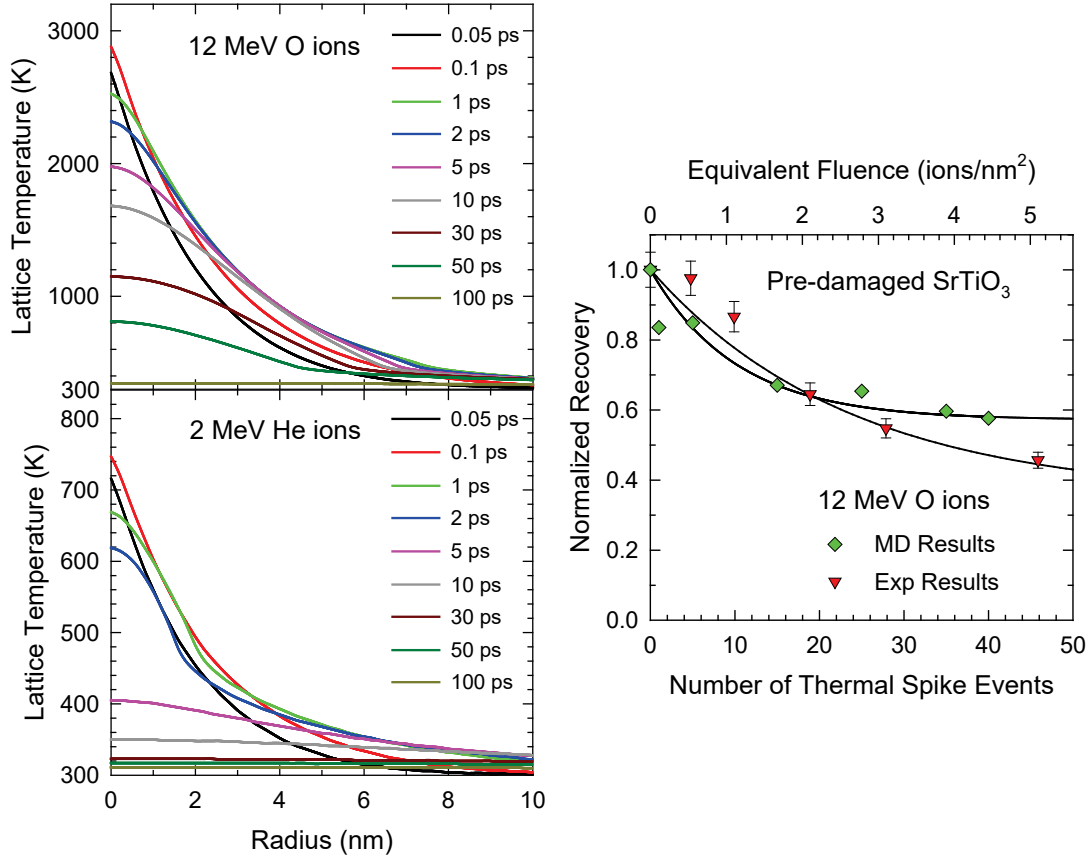


**Fig. 3.** Spatial evolution of lattice temperature with time in pre-damaged SrTiO<sub>3</sub> based on the two-temperature model for (a) 12 MeV O ions and (b) 2 MeV He ions; (c) normalized recovery from MD simulations of thermal spike events for 12 MeV O ions in pre-damaged SrTiO<sub>3</sub> as a function of number of events and equivalent ion fluence, along with experimental results from Fig. 2(a).

The observed recovery in Fig. 2(a) for C and O ions is believed to be driven by inelastic thermal spikes created by the transfer of  $S_e$  to the lattice via electron-phonon coupling. MD simulations coupled with the inelastic thermal spike model were employed to investigate the response of pre-damaged SrTiO<sub>3</sub> to thermal spike events induced by 12 MeV O ions. Using parameters previously developed for pre-damaged SrTiO<sub>3</sub> [3,31,32], the time and radial

dependence of the local lattice temperature predicted by the two-temperature model for 12 MeV O ions is shown in Fig. 3(a). The maximum lattice temperature is about 2880 K at  $\sim 0.1$  ps, and the temperature exceeds 1000 K over a radius of 2.2 nm for 30 ps. Such thermal spikes should be enough to induce defect recovery, since significant defect recovery is experimentally observed in Au-irradiated SrTiO<sub>3</sub> at annealing temperatures up to 900 K [27]. The MD simulations of defect recovery due to individual thermal spike events were performed in a cell containing 3% Frenkel pairs, and thermal spikes were randomly initiated within a projected area of 9 nm<sup>2</sup>, which allowed calculation of an equivalent fluence. Normalized recovery due to MD thermal spikes from 12 MeV O ions is shown in Fig. 3(c) as a function of number of thermal spike events and equivalent fluence. The MD results are in reasonable agreement with the experimental results, also shown, which confirms defect recovery is driven by ionization-induced thermal spikes from C and O ions. The differences between MD and experimental results may be due to deficiencies in empirical potentials, different initial damage states, or uncertainties in two-temperature model parameters.

While recovery for C and O ions is associated with thermal spikes, the local temperature predicted by the two-temperature model for 2 MeV He ions is shown in Fig. 3(b). The maximum lattice temperature is about 750 K at 0.1 ps and rapidly decreases to 400 K after 5 ps. Local heating due to 2 MeV He ions, as well as 200 keV electrons, is not sufficient to cause defect annealing. This is consistent with two distinct regimes of behavior observed in the dependence of recovery cross sections on  $S_e$  in Fig. 4, which are clearly indicated by changes in slope shown by

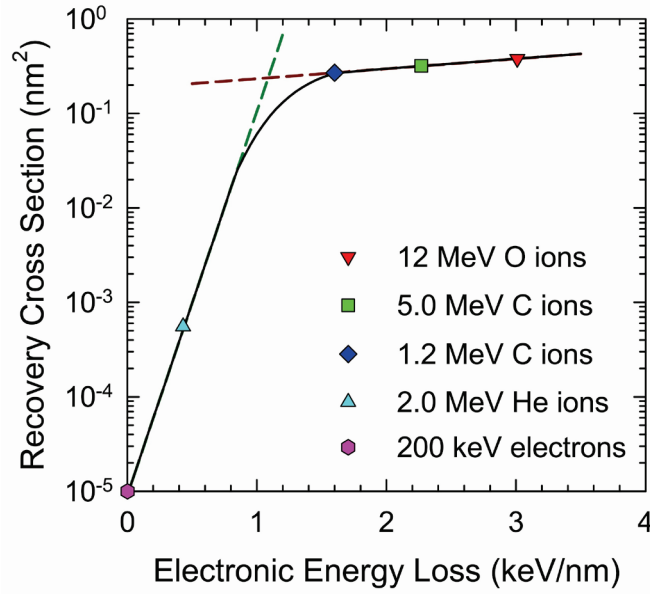


**Fig. 4.** Dependence of ionization-induced recovery cross sections on electronic energy loss,  $S_e$ .

dashed lines. Above a  $S_e$  of 1.1 keV/nm and below the  $S_e$  threshold for track formation ( $\sim 6.5$  keV/nm), the recovery cross sections for C and O ions exhibit a linear dependence on  $S_e$ , similar to that observed in SiC [35]. Below 1.1 keV/nm, the recovery cross sections decrease by several orders of magnitude with decreasing  $S_e$ . The recovery for 2 MeV He ions and 200 keV electrons may be due to longer-lived electronic excitations that can enhance defect mobility, such as the enhanced oxygen vacancy diffusion observed in SrTiO<sub>3</sub> under photo-excitation [36].

In summary, recent studies have shown that above a  $S_e$  threshold of 6.5 keV/nm amorphous tracks are formed in pre-damaged SrTiO<sub>3</sub> due to melt-quenching along the ion track. In this study, the response of pre-damaged SrTiO<sub>3</sub> to  $S_e$  values below this threshold has been investigated using 2 MeV He, 1.2 MeV C, 5 MeV C and 12 MeV O ions. While melt-quenching

does not occur for these ions, the inelastic thermal spike causes enough local heating to induce defect recovery. The results indicate two distinct regimes of ionization-induced recovery with different dominant processes. For C and O ions, with  $S_e$  between 1.6 and 3 keV/nm, the recovery cross sections range from 0.27 to 0.38 nm<sup>2</sup>, and molecular dynamics simulations confirm that the dominant recovery process is driven by highly-localized inelastic thermal spikes created via electron-phonon coupling. Below this  $S_e$  regime, the recovery cross section decreases by several orders magnitude to about  $5.5 \times 10^{-4}$  nm<sup>2</sup> for 2 MeV He ions and  $1.0 \times 10^{-5}$  nm<sup>2</sup> for 200 keV electrons, and the dominant recovery process is believed to be associated with electronic excitations that enhance defect mobility.

### **Acknowledgments**

This work was supported by the U.S. Department of Energy, Office of Science, Basic Energy Sciences, Materials Sciences and Engineering Division under Contract DE-AC05-00OR22725.

The RBS/C analysis was partially supported by the University of Tennessee Governor's Chair program.

### **References**

- [1] S.J. Zinkle, V. Skuratov, D.T. Hoelzer, Nucl. Instrum. Methods Phys. Res. B, 191 (2002) 758-766.
- [2] W.J. Weber, D.M. Duffy, L. Thomé, Y. Zhang, Curr. Opin. Solid State Mater. Sci. 19 (2015)1–11.

- [3] W.J. Weber, E. Zarkadoula, O.H. Pakarinen, R. Sachan, M.F. Chisholm, P. Liu, H. Xue, K. Jin, Y. Zhang, *Sci. Rep.* 5 (2015) 7726.
- [4] N. Sellami, M.L. Crespillo, Y. Zhang, W.J. Weber, *Mater. Res. Lett.* 6 (2018) 339-344.
- [5] G.D. Wilk, R.M. Wallace, J.M. Anthony, *J. Appl. Phys.* 89 (2001) 5243-5275.
- [6] J.H. Haeni, P. Irwin, W. Chang, R. Uecker, P. Reiche, Y.L. Li, S. Choudhury, W. Tian, M.E. Hawley, B. Craigo, A.K. Tagantsev, X.Q. Pan, S.K. Streiffer, L.Q. Chen, S.W. Kirchoefer, J. Levy, D.G. Schlom, *Nature* 430 (2004) 758-761.
- [7] A. Spinelli, M.A. Torija, C. Liu, C. Jan, C. Leighton, *Phys. Rev. B* 81 (2010) 155110.
- [8] W.D. Rice, P. Ambwani, M. Bombeck, J.D. Thompson, G. Haugstad, C. Leighton, S.A. Crooker, *Nat. Mater.* 13 (2014) 481-487.
- [9] D.W. Reagor, V.Y. Butko, *Nat. Mater.* 4 (2005) 593–596.
- [10] P.P. Aurino, A. Kalabukhov, N. Tuzla, E. Olsson, T. Claeson, D. Winkler, *Appl. Phys. Lett.* 102 (2013) 201610.
- [11] S. Matthew, A. Annadi, T.K. Chan, T.C. Asmara, D. Zhan, X.R. Wang, S. Azimi, Z. Shen, A. Rusydi, Ariando, M.B.H. Breese, T. Venkatesan, *ACS Nano* 7 (2013) 10572-10581.
- [12] Y. Liu, Q. Huang, M. Qiao, T.J. Wang, H.L. Song, P. Liu, X.L. Wang, *Nucl. Instrum. Methods Phys. Res. B* 406 (2017) 606-610.
- [13] M. L. Crespillo, J.T. Graham, F. Agulló-López, Y. Zhang, W.J. Weber, *Crystals* 9 (2019) 95.
- [14] S. Glinšek, T. Pečnik, V. Cindro, B. Kmet, B. Rožnič, M. Malič, *Acta Mater.* 88 (2015) 34-40.
- [15] M.G. Cain, P.M. Weaver, M.J. Reece, *J. Mater. Chem A.* 4 (2016) 10394-10402.
- [16] W.J. Weber, A. Navrotsky, S. Stefanovsky, E.R. Vance, E. Vernaz, *MRS Bulletin* 34 (2009) 46-53.

- [17] C. Sabathier, J. Chaumont, J.-C. Krupa, Nucl. Instrum. Methods Phys. Res. B 196 (2002) 308-314.
- [18] Y. Zhang, J. Lian, Z. Zhu, W.D. Bennett, L.V. Saraf, J.L. Rausch, C.A. Hendricks, R.C. Ewing, W.J. Weber, J. Nucl. Mater. 389 (2009) 303-310.
- [19] H. Xue, E. Zarkadoula, P. Liu, K. Jin, Y. Zhang, W.J. Weber, Acta Mater. 127 (2017) 400-406.
- [20] H. Xue, E. Zarkadoula, R. Sachan, Y. Zhang, C. Trautmann, W.J. Weber, Acta Mater. 150 (2018) 351-359.
- [21] M. Karlušić, M. Jakšić, H. Lebius, B. Ban-d'Etat, R.A. Wilhelm, R. Heller, M. Schleberger, J. Phys. Appl. Phys. 50 (2017) 205302.
- [22] W. Li, M.D. Rodriguez, P. Kluth, M. Lang, N. Medvedev, M. Sorokin, J. Zhang, B. Afra, M. Bender, D. Severin, C. Trautmann, R.C. Ewing, Nucl. Instrum. Methods Phys. Res. B 302 (2013) 40-47.
- [23] G. Veliša, E. Wendler, H. Xue, Y. Zhang, W.J. Weber, Acta Mater. 149 (2018) 256-264.
- [24] K. Oyoshi, S. Hishita, H. Haneda, J. Appl. Phys. 87 (2000) 3450-3456.
- [25] Y. Zhang, J. Lian, C.M. Wang, W. Jiang, R.C. Ewing, W.J. Weber, Phys. Rev. B 72 (2005) 1-8.
- [26] Y. Zhang, M.L. Crespillo, H. Xue, K. Jin, C.H. Chen, C.L. Fontana, J.T. Graham, W.J. Weber, Nucl. Instrum. Methods Phys. Res. B 338 (2014) 19-30.
- [27] S. Thevuthasan, W. Jiang, V. Shutthanandan, W.J. Weber, J. Nucl. Mater. 289 (2001) 204-209.
- [28] J.F. Ziegler, J.P. Biersack, ULittmark, The Stopping and Range of Ions in Solids, Pergamon, New York, 1985.
- [29] W.J. Weber, Y. Zhang, Curr. Opin. Solid State Mater. Sci (2019).  
<https://doi.org/10.1016/j.cossms.2019.06.001>

- [30] M. Toulemonde, W. Assmann, C. Dufour, A. Meftah, F. Studer, C. Trautmann, *Mat. Fys. Medd. K. Dan. Vidensk. Selsk.* 52 (2006) 263-292.
- [31] E. Zarkadoula, O.H. Pakarinen, H. Xue, Y. Zhang, W.J. Weber, *Phys. Chem. Chem. Phys.* 17 (2015) 22538-22542.
- [32] E. Zarkadoula, H. Xue, Y. Zhang Y, W.J. Weber, *Scripta Mater.* 110 (2016) 2-5.
- [33] I.T. Todorov, W. Smith, K. Trachenko, M.T. Dove, *J. Mater. Chem.* 16 (2006) 1911-1918.
- [34] M.A. McCoy, R.W. Grimes, W.E. Lee, *Philos. Mag. A* 75 (1997) 833-846.
- [35] Y. Zhang, H. Xue, E. Zarkadoula, R. Sachan, C. Ostrouchov, X. Wang, S. Zhang, T.S. Wang, W.J. Weber, *Curr. Opin. Solid State Mater. Sci.* 21 (2017) 285-298.
- [36] Y. Li, Y. Lei, B.G. Shen, J.R. Sun, *Sci Rep.* 5 (2015) 14576.